

Processability of K340 Cold Work Tool Steel by Directed Energy Deposition Technique

Original

Processability of K340 Cold Work Tool Steel by Directed Energy Deposition Technique / Kenevisi, Ms; Martelli, Pa; Gobber, Fs; Ugues, D; Biamino, S. - In: IOP CONFERENCE SERIES: MATERIALS SCIENCE AND ENGINEERING. - ISSN 1757-8981. - 1310:(2024). [10.1088/1757-899x/1310/1/012021]

Availability:

This version is available at: 11583/2992032 since: 2024-08-29T08:22:32Z

Publisher:

IOP Science

Published

DOI:10.1088/1757-899x/1310/1/012021

Terms of use:

This article is made available under terms and conditions as specified in the corresponding bibliographic description in the repository

Publisher copyright

(Article begins on next page)

PAPER • OPEN ACCESS

Processability of K340 Cold Work Tool Steel by Directed Energy Deposition Technique

To cite this article: MS Kenevisi *et al* 2024 *IOP Conf. Ser.: Mater. Sci. Eng.* **1310** 012021

View the [article online](#) for updates and enhancements.

You may also like

- [Effect of hot isostatic pressing on the microstructure of laser powder bed fused A20X™ alloy](#)
J Barode, E Bassini, A Aversa et al.
- [Applying lab-based DCT to reveal and quantify the 3D grain structure of a miniature chess rook produced by binder jetting](#)
J Sun, F Bachmann, J Oddershede et al.
- [The effect of processing parameters on dislocation density and tensile properties in laser powder bed fusion 316L](#)
M Schreiber, C Brice, K Findley et al.

PRIME
PACIFIC RIM MEETING
ON ELECTROCHEMICAL
AND SOLID STATE SCIENCE

HONOLULU, HI
October 6-11, 2024

Joint International Meeting of
The Electrochemical Society of Japan
(ECS)
The Korean Electrochemical Society
(KECS)
The Electrochemical Society (ECS)

Early Registration Deadline:
September 3, 2024

**MAKE YOUR PLANS
NOW!**

Processability of K340 Cold Work Tool Steel by Directed Energy Deposition Technique

MS Kenevisi^{1,2,*}, PA Martelli^{1,2}, FS Gobber^{1,2}, D Ugues^{1,2} and S Biamino^{1,2}

¹ Department of Applied Science and Technology (DISAT), Politecnico di Torino, Italy

² Integrated Additive Manufacturing iAM@PoliTO Center, Politecnico di Torino, Italy

*E-mail: saleh.kenevisi@polito.it

Abstract. Directed Energy Deposition (DED) is an additive manufacturing process which can be used to repair defected components, such as blanking dies made of K340 tool steel. In this work, double tracks of K340 steel were deposited using DED process to study the processability of the alloy, and the tracks were characterized by light optical microscopy (LOM), scanning electron microscopy (SEM) and microhardness test. The results showed that near full-dense deposits can be made. However, the thermal cycle imposed by the process alters the microstructure of the material. Further investigation is required to make it possible to achieve a more homogeneous microstructure.

1. Introduction

Directed Energy Deposition (DED) is an additive manufacturing (AM) process that involves accurately depositing material onto a substrate by using a focused energy source, such as electron beam or laser. The process involves melting or sintering a feedstock material, which may be in the form of powder or wire, onto the substrate's surface layer-by-layer [1]. This process has been used both for fabricating new components and repairing damaged parts [2,3]. The processing parameters in each AM process have a significant impact on the quality of the fabricated components. Chen et al. [4] and Cho et al. [5] investigated how processing parameters can affect the deposition process and the microstructure of the material. Additionally, different studies have been conducted to investigate and to improve the effectiveness of the DED repairing approach for various alloys, such as steels [6], Ti [7], and Ni [8] alloys.

K340 tool steel, also known as Böhler K340 ISODUR, is a high-carbon and high-chromium tool steel widely used for cold work applications because of its well-balanced properties. It possesses high hardness and wear resistance, improved toughness, and dimensional stability [9]. It is widely used as blanking tools and dies. However, with time, defects such as wear or cracking may occur on the dies.

The use of the powder-fed DED process for depositing K340 steel provides the capability to repair damaged parts. However, the DED repair process may modify the microstructure of the component. Generally, high-carbon steels are not considered as suitable alloys for AM processes because of their high susceptibility to cracking [10]. This study investigates the DED processability of the alloy, which, to the authors' knowledge, has not been previously examined in the literature. The study examines how processing parameters impact the geometry and the microstructure of the deposits.



2. Materials and Methods

The material used in this study was BÖHLER K340 Isodur powder particles. As the powder particles of this material is not commercially available, HERMIGA 100/10 VI gas atomizer by PSI was used to produce the powder. The obtained powder was then sieved to obtain a particle size range of 45-125 μm with D50 = 87.8 μm . In terms of the powder characteristics, the particles were generally spherical with some satellites attached to them, as can be seen in figure 1(a). The cross-section analysis of the particles (figure 1(b)) also did not reveal high amounts of internal gas pores.

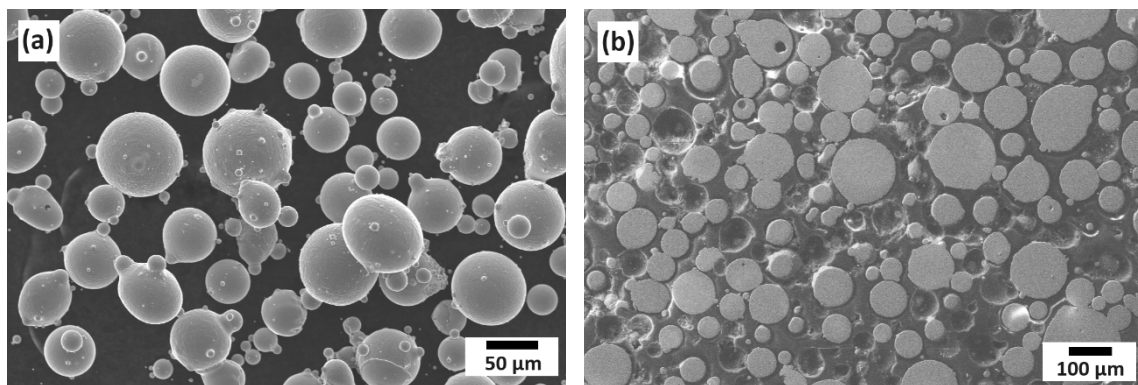


Figure 1. SEM micrographs of a) particles and b) cross-section of the powder particles used in this work.

The chemical composition of the powder was analyzed by LECO ONH836 and CS844 instruments and a ZEISS EVO 15 scanning electron microscope equipped with Ultim Max EDS detector by Oxford Instruments. The results of the alloying elements are provided in table 1, which is comparable to the nominal composition provided by Böhler.

Table 1. Chemical composition (wt.%) of the produced powder.

Element	C	Cr	Mo	V	Si	Mn	Al	Nb
Powder	1.12	8.05	1.91	0.42	0.81	0.46	0.89	0.16

Fifteen double-tracks with different sets of processing parameters (nozzle travel speed from 400 to 700 mm/min, laser powder from 500 to 900 W, and carrier gas flow rate from 4.5 to 7.5 l/min) were deposited on a K340 platform by Laserdyne 430 laser metal deposition machine by Prima Additive equipped with 1 kW Yb laser with a spot size of 2 mm.

The cross-sections of the deposits were studied by SEM. Moreover, the hardness measurement was done by using VMHT 1200 Leica Vickers microhardness tester and applying 300 g force with a dwell time of 15 s.

3. Results and Discussion

3.1 Single Tracks Morphology

The morphology of different deposits was studied, and the results for three samples are illustrated in figure 2. It can be seen that by increasing the energy density both the width and the height of the deposit increases. At $S = 700$ mm/min and $P = 500$ W (sample A) the average height and the

width of the deposit are 214.6 μm and 2.47 mm, respectively. By decreasing the nozzle speed to 550 mm/min and increasing laser power to 700 W (sample B), an increase in the height of the track to 300.6 μm and width of it to 2.84 mm was observed. Further increasing the energy density ($S = 400$ mm/min and $P = 900$ W) resulted in a track with 682.5 μm of height and 2.89 mm of width (sample C).

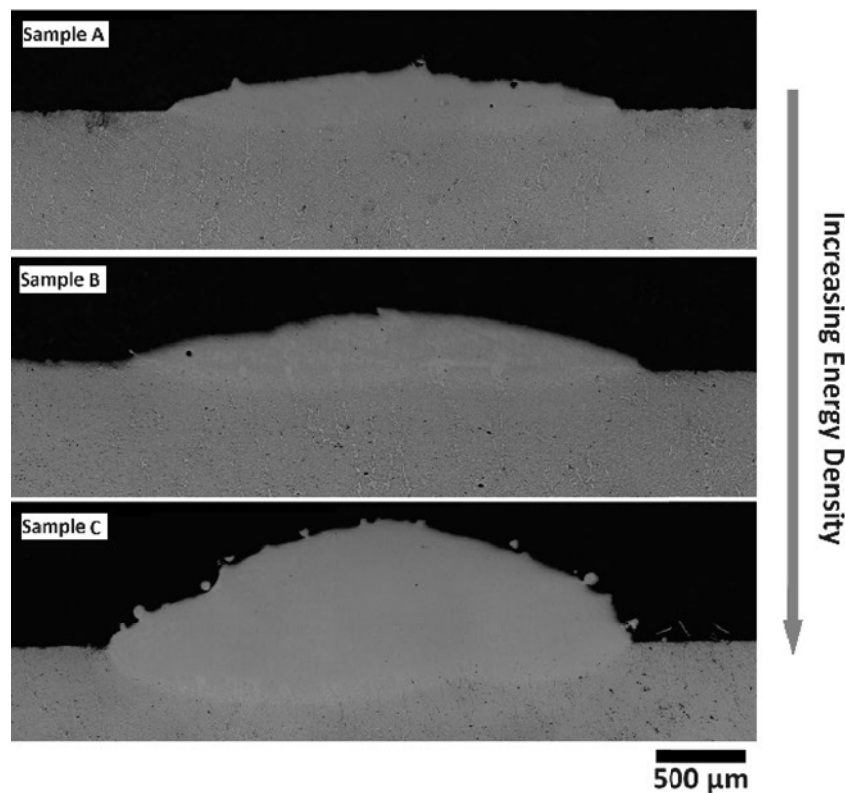


Figure 2. LOM micrographs of the deposits illustrating the tracks' morphology.

This is because by lowering the travel speed and increasing the laser power, the temperature of the melt pool increases and more powder particles are deposited and incorporated into the melt pool [11,12]. It was also observed that the sample with the highest energy density had the biggest deposit. Moreover, it showed the highest value of dilution which is 26%. However, on the other side, the dilution of the track deposited with the highest travel speed and lowest laser power was only 5%. Deeper penetration of the material can be achieved by the elevated melt pool temperature at high laser powers [13]. The statistical analysis showed that the laser powder was the most significant factor among the three parameters that affects the dilution. Generally, dilution values between 10 – 30 % are desired in the literature [14].

3.2 Defects and Microstructural Evolution

The porosity content of the deposits was measured from different cross-sections of each sample and the average value for samples A, B, and C were 0.5, 0.3, and 0.1%, respectively. The cross-section analysis did not disclose any lack of fusion (LOF) defect in all the samples. The declining trend in the porosity content by increasing the energy density the melt pool is remained at higher temperature and longer times before solidification. Therefore, more gases, which were within the powder particles or generated due to the evaporation of elements, that are entrapped in the melt pool can escape and reach the surface.

Regarding the microstructural evolution, depositing the material caused a modification in the microstructure of the material, which occurred in all depositions. To represent this modification, figure 3 depicts the SEM micrograph of sample C. As can be seen, the microstructure of the deposit differs from that of the substrate and there is a heat affected zone (HAZ) as well. The microstructure of the deposited material is characterized by a fine equiaxed cellular structure. EDS analysis suggested the segregation of elements such as C, Cr, Mo, and V at cell boundaries as well as the presence of austenite.

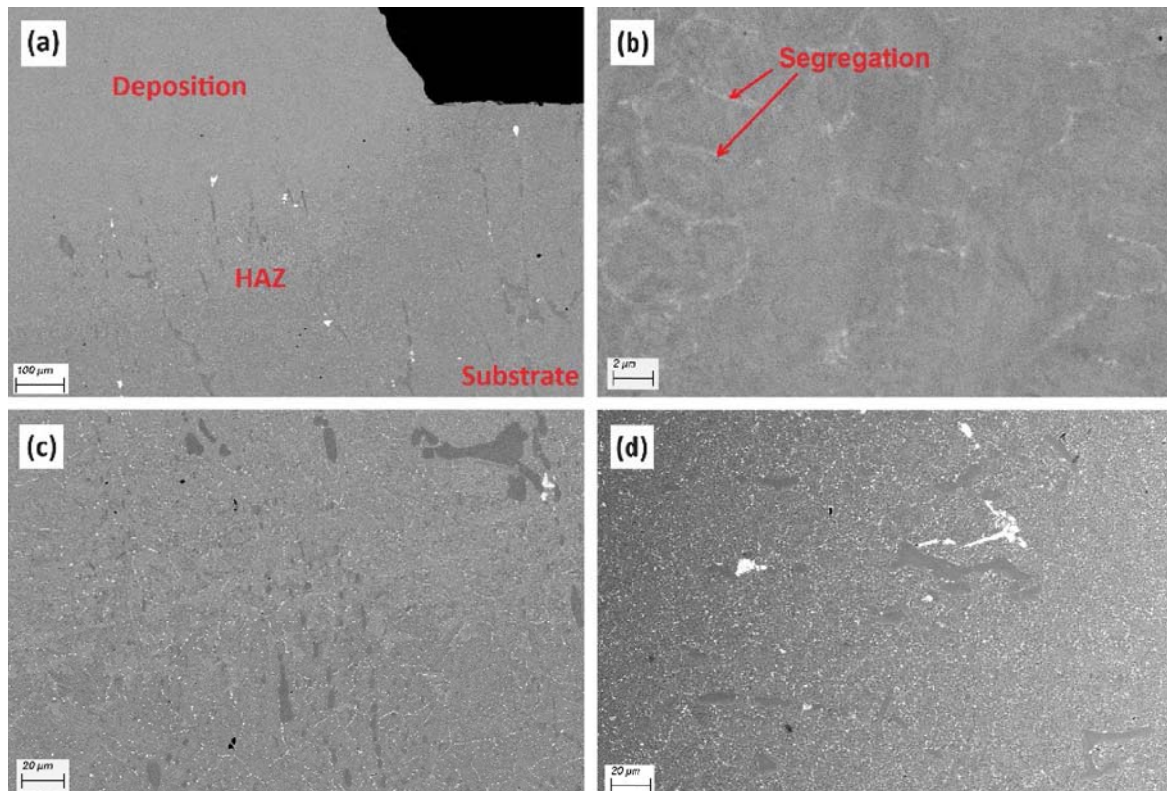


Figure 3. SEM micrographs from the cross-sections of sample C illustrating the microstructure of a) all regions at low magnification, b) deposit, c) HAZ, and d) substrate material.

On the other side, the substrate was used in an annealed condition and both spheroidized and elongated carbides were dispersed in a ferritic matrix. The big blocky bright regions are also carbides rich in Nb. Due to the applied thermal cycle that the material close to the deposition has experienced, an HAZ was identified. In this region, fine carbides are precipitates along the grain boundaries. These carbides were rich in Cr and Mo. Compared to the microstructure of the substrate, there was no evidence of fine spherical carbides (gray carbides sized 1-3 µm). This is due to the dissolution of these carbides at relatively high temperatures imposed to this region.

3.3 Hardness Measurement

Vickers Microhardness test was performed on a $1200 \times 1200 \mu\text{m}^2$ area consisting all different regions. The hardness map was produced and illustrated in figure 4. It shows that the HAZ close to the deposition possesses the highest hardness value. The hardness in this region reaches up to 690 HV, while the corresponding values for the base metal and the deposit are within the range of 240-300 and 390-440 HV, respectively.

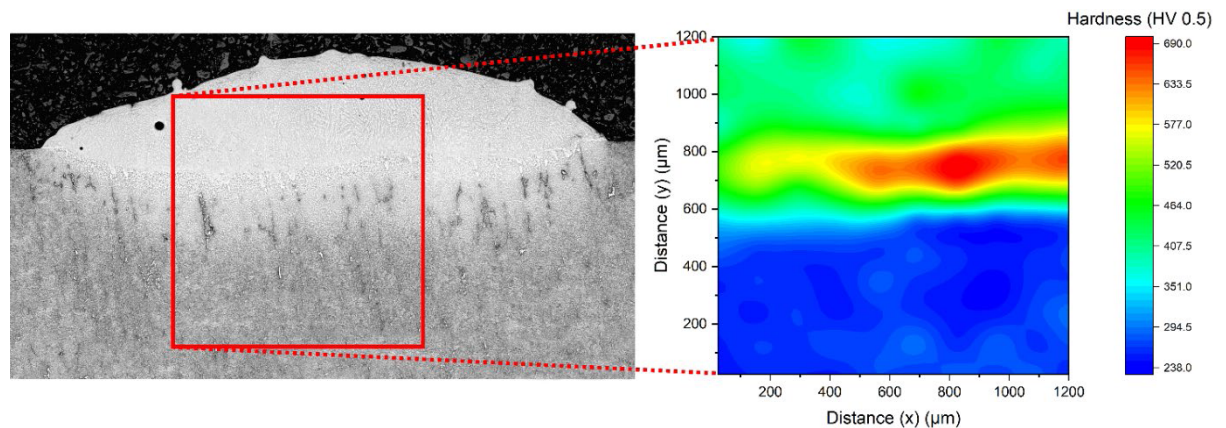


Figure 4. Microhardness map of the selected region of sample C.

The high hardness value of the HAZ close to the deposit suggests that the material in this region may reach the austenitizing temperature during the deposition process. In the cooling stage, the microstructure transformed to martensite and the primary carbides, which are responsible for the increased hardness [15].

4. Conclusions

In this study, a preliminary investigation of the processability of K340 cold work tool steel by DED process was conducted. Double tracks were deposited with different sets of processing parameters. The results showed that by increasing laser power and decreasing nozzle travel speed, in other words increasing the energy density, both height and width of the deposits increased. Laser power was shown to be the most significant factor affecting the morphology of the tracks. Microstructural analysis revealed the presence of retained austenite and segregation of alloying elements in the deposited material. Moreover, the applied thermal cycle introduced some HAZs with modified microstructures. Hardness measurement also confirmed the different microstructures of the substrate, HAZ, and the deposited material. More in-depth microstructural analysis is going to be performed in future works.

References

- [1] Vafadar A, Guzzomi F, Rassau A and Hayward K 2021 *Appl Sci* **11** 1–33
- [2] Kim T G and Shim D S 2021 *Mater Sci Eng A* **828** 142004
- [3] Piscopo G and Iuliano L 2022 *Int J Adv Manuf Tech* **119** 6893–6917
- [4] Chen B, Huang Y, Gu T, Tan C and Feng J 2018 *Rapid Prototyp J* **24** 964–972
- [5] Cho K T, Nunez L, Shelton J and Sciammarella F 2023 *J Manuf Mater Process* **7** 105
- [6] Simoneau L, Bois-Brochu A and Blais C 2020 *J Mater Eng Perform* **29** 6139–6146
- [7] Rauch M, Hascoet J-Y and Mallaiah M 2020 *MATEC Web Conf.* **321** 3017
- [8] Wilson J M, Piya.C, Shin Y C, Zhao F and Ramani K 2014 *J Clean Prod* **80** 170–178
- [9] Jovicevic-Klug P, Toth L and Podgornik B 2022 *Coatings* **12** 1296
- [10] Vincic J, Aversa A, Lombardi M and Manfredi D 2023 *Met Mater Int* **30** 501-516
- [11] Peyre P, Aubry P, Fabbro R, Neveu R and Longuet A 2008 *J Phys D Appl Phys* **41** 025403
- [12] Hua T, Jing C, Xin L, Fengying Z and Weidong H 2008 *J Mater Process Tech* **198** 454–462

- [13] Félix-Martínez C, Ibarra-Medina J, Fernández-Benavides D A, Cáceres-Díaz L A and Alvarado-Orozco J M 2021 *Int J Adv Manuf Tech* **115** 3999–4020
- [14] Ahn D G 2021 *Int J Pr Eng Man-Gt* **8** 703–742
- [15] Zhang X, Liu W, Sun D and Li Y 2007 *Metall Mater Trans A* **38** 499–505